FRCM/SRG strengthened masonry in diagonal compression: experimental results and analytical approach proposal

FRCM/SRG strengthened masonry in diagonal compression: experimental results and analytical approach proposal

Francesca Ferretti[a,*], Claudio Mazzotti[a]

[a] *Department of Civil, Chemical, Environmental and Materials Engineering, University of Bologna, Viale Risorgimento 2, 40136 Bologna, Italy*
* Corresponding author. Tel.: +39 051 2093246
E-mail addresses: francesca.ferretti10@unibo.it; claudio.mazzotti@unibo.it.

Abstract

The in-plane shear behavior of masonry panels strengthened with Fiber Reinforced Cementitious Matrices (FRCM) or Steel Reinforced Grouts (SRG) is investigated in this research in order to propose an improved analytical approach able to predict the maximum capacity. With this purpose, a dedicated experimental campaign is developed through the execution of diagonal compression tests. Experimental outcomes highlight the crucial role of the mortar matrix in enhancing the shear capacity of the masonry panels. The careful analysis of the different contributions during the tests allows the development of predictive formulas taking into account the role of the matrix and of the cracked masonry.

Keywords: brick masonry, diagonal compression tests, in-plane shear behavior, FRCM/SRG strengthening systems, analytical formulation.

1 Introduction

The great damages experienced by existing masonry buildings during past earthquakes [1–3] highlighted the seismic vulnerability of these construction typologies [4–6] and the need of designing efficient strengthening interventions to improve their structural behavior in presence of horizontal actions. Nowadays, fiber reinforced composite materials are increasingly used for this purpose. Compared to traditional retrofitting techniques, e.g. welded steel meshes embedded in thick (more than 30 mm) cementitious mortar layers, these strengthening solutions aim at the enhancement of the structural capacity, both in-plane and out-of-plane, without determining significant changes in the

mass and stiffness distributions of the buildings [7,8]. Therefore, high-performance materials, such as unidirectional or bidirectional high-strength long fibers, are applied to the structural elements embedded inside inorganic or organic matrix layers, characterized by a reduced thickness.

The first composite strengthening solution introduced consisted in the application of Fiber Reinforced Polymers (FRP) over the surfaces of masonry walls [9–12]. This technique involves the use of fibers, made of different materials, embedded into an organic matrix, i.e epoxy resin. Experimental campaigns performed for the mechanical characterization of FRP systems, demonstrated a good tensile and bond behavior of these materials when applied to masonry elements [13–19]. However, some critical issues can be associated with the use of FRPs, mainly related to the use of organic matrices: the poor compatibility with the masonry substrate, the lack of vapor permeability and the weak behavior at high temperatures. More recently, to partially overcome these drawbacks, Fiber Reinforced Cementitious Matrices (FRCM) and Steel Reinforced Grouts (SRG) were introduced, based on the replacement of the epoxy resin with an inorganic matrix, either cement-based or lime-based mortar. Strengthening interventions with FRCM and SRG systems resulted to be more compatible with the masonry substrate and more reversible with respect to the ones involving the use of FRPs [20–22].

The mechanical behavior of FRCM and SRG composite systems, denoted in the following as "composite systems" or "strengthening systems" for simplicity, is significantly different if compared to FRPs, due to the diverse nature and performances of the matrix. Therefore, several studies on the tensile and bond properties of such systems were conducted, identifying a wider range of possible failure modes [23–28]. More in detail, different strengthening solutions were analyzed given that many types of reinforcing fibers can be adopted, depending on the material (e.g. carbon, glass, basalt, steel, PBO, aramid, etc.), the arrangement (e.g. unidirectional or bidirectional, continuous or discontinuous) and the compatibility with the matrix [29–32]. In parallel, experimental campaigns were also performed to study the structural behavior of full-scale masonry samples strengthened by composite systems [33–36]. With reference to the in-plane shear behavior, which is the focus of the

present paper, researches were carried out to study the efficiency of these systems when applied on different masonry typologies, such as brick [37–40], tuff [41–44] and stone [45–47] masonry. Results showed the great effectiveness of the composite systems in enhancing the shear behavior of masonry elements, both in terms of capacity and ductility. The durability of these strengthening materials is currently under investigation, given that they can be susceptible to the degradation of their mechanical properties when subject to particular environmental conditions [48–50].

The large amount of research carried out on these strengthening techniques allowed the formulation of specific Standards or Guidelines, whose main purpose was to give indications about the features of these systems, the field of application, the determination of design material properties, and to propose analytical formulations for the capacity prediction of strengthened elements. They were first developed for FRP [51], while only in recent years specific regulations were introduced also for FRCM and SRG [52–54]. The approach proposed by these Standards for the determination of the in-plane shear capacity of a strengthened panel is an additive approach, based on the evaluation of the masonry and the fibers contributions. On one hand, the proposed analytical formulations were validated through comparisons with experimental results, obtaining a good agreement [40,46,55]. On the other hand, several experimental studies highlighted the fundamental role of the mortar matrix in the enhancement of the shear capacity of masonry [39,56–59], which is not taken into account by the available formulations. Some of these works were carried out on Composite Reinforced Mortar (CRM) systems and led to the proposal of an analytical prediction which explicitly included the mortar matrix contribution [57,59,60]. CRM systems are characterized by a greater mortar matrix thickness (more than 15 mm) and by a larger bundle spacing with respect to FRCM and SRG composite systems. The global behavior of the strengthening systems is similar, even if local differences can be observed.

The present paper aims to present a study regarding the shear behavior of FRCM/SRG strengthened clay brick masonry panel. More in detail, two masonry typologies, characterized by different material properties and bond patterns, were strengthened by distinct composite systems and

were subject to diagonal compression tests. This test is indeed one of the most adopted setups for the study of the shear behavior of masonry panels, given its relatively simple execution. Based on the experimental results from different composite systems, which included also complete materials characterization, it was possible to properly investigate and analyze the main phases of the mechanical behavior of strengthened masonry panels subject to in-plane shear, and the specific role of each component (i.e. masonry, mortar matrix and reinforcing fibers). This original and detailed analysis, carried out and explained in the paper, allowed to propose, calibrate and validate an improved alternative analytical approach, inspired by the cited proposals [57,59,60], applicable for the determination of the shear strength capacity expected for FRCM/SRG strengthened masonry panels.

2 Existing design provisions for FRCM/SRG strengthened masonry panels

The development of national and international Standards or Guidelines for the design of strengthening interventions on masonry walls using composite systems is relatively new, since the use of these materials has gained importance and diffusion in recent years. In the American and in the European framework, specific design provisions for FRCM and SRG systems have been formulated and included in international technical Guidelines [52,53], which will be referred in the following as ACI, RILEM and CNR Italian Guidelines. Concerning the strengthening of masonry walls subject to in-plane loads, a similar design approach is reported in all the cited documents.

Regarding shear-controlled failure mode, the in-plane shear capacity of a FRCM/SRG strengthened masonry panel ($V_{t,R}$) is determined by adding the contribution of the reinforcement to the shear resistance of the unreinforced masonry wall, according to the equation:

$$V_{t,R} = V_t + V_{t,f}\,, \tag{1}$$

where V_t is the plain masonry shear contribution and $V_{t,f}$ is the fibers shear contribution. The former should be evaluated considering the minimum shear capacity of the masonry panel, according to the possible shear failure modes for an unreinforced masonry wall. The latter can be calculated with Equations (2-4), according to the ACI, RILEM and CNR Italian Guidelines, respectively:

$$V_{t,f} = \phi_s \cdot n_f \cdot A_f \cdot E_f \cdot \varepsilon_{fd}\,, \tag{2}$$

$$V_{t,f} = \gamma_k \cdot n_f \cdot A_f \cdot E_f \cdot \varepsilon_{fd}\,, \tag{3}$$

$$V_{t,f} = \frac{1}{\gamma_{Rd}} \cdot n_f \cdot A_f \cdot \alpha_t \cdot E_f \cdot \varepsilon_{fd}\,, \tag{4}$$

where n_f is the number of layers, A_f is the area of the grid reinforcement, E_f is the stiffness of the cracked FRCM/SRG system (ACI) or the dry fiber elastic modulus (RILEM, CNR), and ε_{fd} is the design strain of the composite system. Details and limitations about the evaluation of the reinforcement area A_f are reported in the Guidelines, e.g. in case of continuous or discontinuous strengthening system. The coefficients γ_k and γ_{Rd} are safety factors, equal to 0.5 and 2, respectively, while ϕ_s is a strength reduction factor for shear and α_t is a coefficient accounting for a reduced tensile strength for fibers subject to shear, both equal to 0.8.

The expressions reported in Equations (2-4) are conceptually equivalent, since the FRCM/SRG contribution is based, in all cases, on the evaluation of the maximum load that the reinforcing fibers can carry, calculated as the maximum design strength ($E_f \cdot \varepsilon_{fd}$) multiplied by the area of the fiber reinforcement effective in shear. The only differences are related to the values assigned to the safety factors or to the strength reduction factors. All the Guidelines include specific indications for the evaluation of the design strain ε_{fd}, which should be determined by considering different factors: (i) results of tensile and bond tests performed for the mechanical characterization of the composite systems; (ii) expected failure mode, e.g. end or intermediate delamination; (iii) design safety factors. Moreover, in case of asymmetric application of the strengthening system (e.g. only on one side of a masonry wall), the effects of eccentricity should be adequately considered by reducing the reinforcement shear contribution $V_{t,f}$ of the 30% at least.

3 Materials and methods

The experimental campaign presented in the paper consisted in performing diagonal compression tests on brick masonry panels strengthened by means of composite systems. Two masonry typologies were considered, denoted as *A* and *B* in the following, for a total of 17 brick masonry samples, built by using the same clay bricks and two different mortar mixes. With the objective of analyzing the efficiency of different composite systems in improving the shear behavior of existing masonry walls, variations in the masonry bond pattern, in the constituent materials and in the strengthening layouts were considered.

The masonry samples were built to reproduce bond patterns typically observed in the Italian built heritage. More in detail, double-wythe brick masonry panels were constructed in laboratory with three different bond patterns: Flemish bond (Figure 1*a,b*), header bond (Figure 1*c*) and a Flemish bond pattern, denoted as "false Flemish" in the following, characterized by the lacking of transversal connection between the wall wythes, and realized by cutting the transversal bricks (Figure 1*d*).

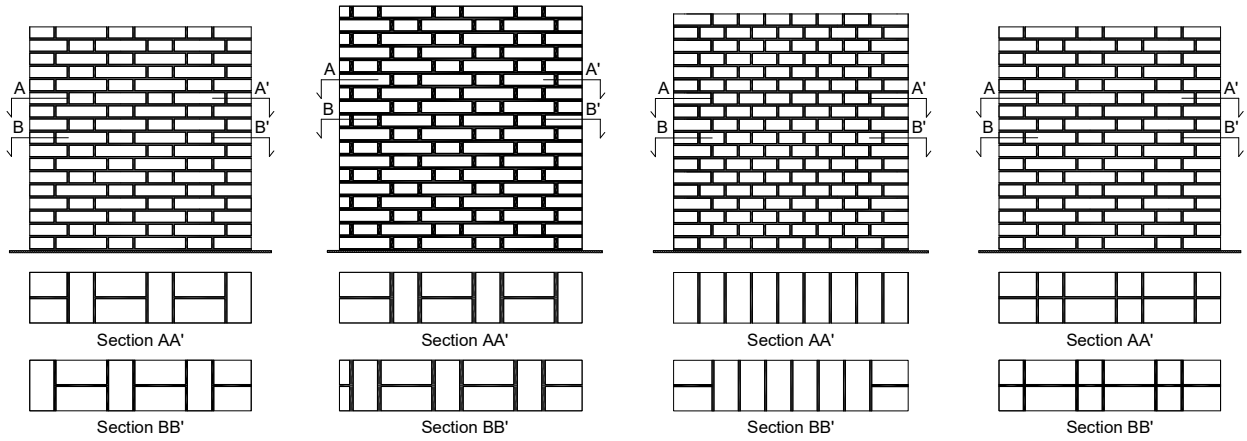

Figure 1. Masonry bond patterns: (a) Flemish bond *A*; (b) Flemish bond *B;* (c) header bond; (d) false Flemish bond.

After 28 days of curing in laboratory environment, the samples were strengthened by using bidirectional grid reinforcements or unidirectional fiber strips, which were applied symmetrically, on both sides of the masonry panels, adopting the following strengthening layouts:

- Continuous layout (Figure 2*a*): bidirectional basalt or aramid-glass systems were applied on the entire surfaces of 10 samples as single-layer or double-layer reinforcements; in the first case, a

total matrix thickness of 6 mm per side was used; in the second case, considered only for one sample strengthened with bidirectional aramid-glass grids, two superimposed grids were embedded within the mortar matrix obtaining an overall thickness of the FRCM system equal to 8 mm per side.

- Discontinuous layout (Figure 2*b,c*): unidirectional steel fiber strips (SRG) were applied on 3 samples, using two configurations, characterized by different strip width and spacing; in particular, the configuration reported in Figure 2*b* was adopted on one sample of the masonry typology *A*, while the configuration shown in Figure 2*c* was applied on two samples of the masonry typology *B*. The overall thickness of the mortar matrix for discontinuous layouts was equal to 6 mm per side.

Mechanical anchorages were adopted on 5 specimens of the masonry typology *A* to prevent end debonding/delamination phenomena and to provide transversal connection.

The characteristics of the tested samples are summarized in Table 1. Notation used to identify the specimens indicates: (i) the bond pattern (*B* = brick, *F* = Flemish bond, *H* = header bond, *FF* = false Flemish bond); (ii) the masonry typology (*A* or *B*, as already introduced); (iii) the adopted grid or strip reinforcements (basalt grids B1 or B2, aramid-glass grid AG, steel fibers S1 or S2); (iv) the presence of mechanical anchorages (*MA*). Four brick masonry panels, one for each masonry typology and bond pattern, were left unreinforced.

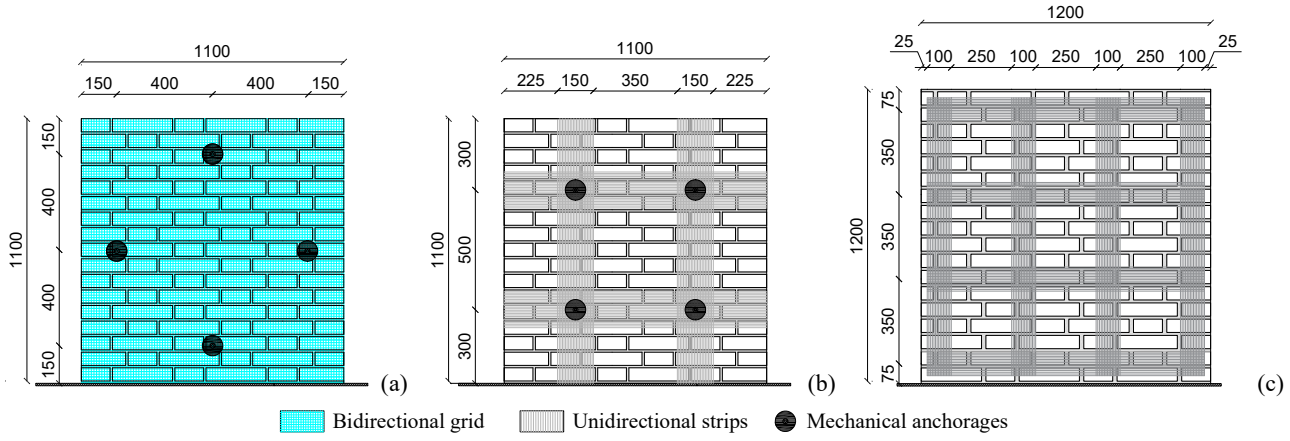

Figure 2. Strengthening layouts: (a) continuous layout; (b) discontinuous layout used for the masonry typology *A*; (c) discontinuous layout used for the masonry typology *B*.

Table 1. Characteristics of the tested brick masonry panels.

Sample code	Dimensions (mm^3)	Bond pattern	Mortar type	FRCM system*	Matrix type	Fiber type	Mechanical Anchorages
B-F_A_URM	1100×1100×250	Flemish bond	NHL1	-	-	-	-
B-F_A_B1	1095×1095×250	Flemish bond	NHL1	C, SL	NHL3	Basalt grid	No
B-F_A_B1-MA	1095×1095×250	Flemish bond	NHL1	C, SL	NHL3	Basalt grid	Yes
B-F_A_B2-MA	1095×1095×250	Flemish bond	NHL1	C, SL	NHL3	Basalt grid	Yes
B-F_A_S1-MA	1090×1105×250	Flemish bond	NHL1	D, SL	NHL3	Steel strips	Yes
B-H_A_URM	1155×1155×250	Header bond	NHL1	-	-	-	-
B-H_A_B1	1160×1160×250	Header bond	NHL1	C, SL	NHL3	Basalt grid	No
B-H_A_B1-MA	1160×1160×250	Header bond	NHL1	C, SL	NHL3	Basalt grid	Yes
B-FF_A_URM	1095×1100×250	False Flemish	NHL1	-	-	-	-
B-FF_A_B1-MA	1095×1100×250	False Flemish	NHL1	C, SL	NHL3	Basalt grid	Yes
B-F_B_URM	1205×1205×250	Flemish bond	NHL2	-	-	-	-
B-F_B_B1	1200×1215×250	Flemish bond	NHL2	C, SL	NHL4	Basalt grid	No
B-F_B_B2	1200×1200×250	Flemish bond	NHL2	C, SL	NHL4	Basalt grid	No
B-F_B_AG-1	1200×1200×250	Flemish bond	NHL2	C, SL	NHL4	Aramid-glass grid	No
B-F_B_AG-2	1205×1200×250	Flemish bond	NHL2	C, DL	NHL4	Aramid-glass grid	No
B-F_B_S1	1205×1210×250	Flemish bond	NHL2	D, SL	NHL4	Steel strips	No
B-F_B_S2	1200×1200×250	Flemish bond	NHL2	D, SL	NHL4	Steel strips	No

* C: continuous layout, D: discontinuous layout, SL: single layer, DL: double layer.

3.1 Bricks

The bricks adopted for the construction of the specimens were fired-clay bricks (120×250×55 mm^3). Standard laboratory tests were performed for the evaluation of their mechanical properties. In particular, 12 uniaxial compressive tests [61] and 12 Brazilian tests [62] were performed on cylindrical samples, having a diameter of 50 mm and characterized by a unitary aspect ratio, obtaining the brick compressive strength $f_{c,b}$ and tensile strength $f_{t,b}$, equal to 18.66 MPa (CoV = 5.3%) and 3.14 MPa (CoV = 15.3%), respectively. Moreover, 5 three-points bending tests [63] were conducted on

prismatic specimens, having dimensions 40×40×250 mm^3, for the determination of the brick flexural strength $f_{fl,b}$, which resulted to be equal to 4.79 MPa (CoV = 6.9%). The elastic modulus of the bricks was determined by performing cyclic compression tests on cylindrical specimens [64], characterized by an aspect ratio equal to 2.5, and it was equal to 6846 MPa (CoV = 3.9%).

3.2 Mortars

In the experimental program, two mortar typologies were adopted for the construction of the brick masonry panels (NHL1 and NHL2) and two mortar typologies were used as matrices of the FRCM systems investigated (NHL3 and NHL4). They were all pre-mixed natural hydraulic lime-based mortars and they were subject to standard laboratory tests for their mechanical characterization. More in detail, prismatic specimens, having dimensions of 160×40×40 mm^3, were prepared and cured as prescribed by the Standard [65]. Six specimens were prepared for each masonry panel: three specimens made of the mortar used for the construction of the panel and three specimens made of the mortar matrix. They were firstly subject to three-points bending tests. Afterwards, uniaxial compression tests were performed on the specimens resulted from the previous test. Cyclic compression tests [64] were also performed on three standard prismatic specimens for each mortar typology to evaluate the elastic modulus. The obtained mechanical properties, in terms of mortar compressive strength $f_{c,m}$, flexural strength $f_{fl,m}$ and elastic modulus E_m, are reported in Table 2.

Table 2. Mechanical properties of the mortars.

Mortar	$f_{c,m}$ (MPa)	CoV (%)	$f_{fl,m}$ (MPa)	CoV (%)	E_m (MPa)	CoV (%)
NHL1	4.8	12.5	1.5	15.1	4586	17.3
NHL2	2.6	12.3	1.2	8.6	4248	18.2
NHL3	12.6	9.5	2.9	22.6	9100	13.8
NHL4	7.1	5.2	3.4	4.8	8675	11.1

It is important to mention that all the tests were conducted at the same age in which the wall panels were tested. Worth noticing that the mortar matrices (NHL3 and NHL4) were characterized by better performances with respect to the mortars used for bedjoints, maintaining at the same time a good compatibility with the masonry substrate.

3.3 Grid and strip reinforcements

The FRCM/SRG systems chosen for the strengthening of the brick masonry panels involved five different types of grid or strip reinforcements:

- Basalt grid B1 (Figure 3*a*): bidirectional balanced basalt grid characterized by a weight density of 200 g/m^2, a nominal bundle spacing equal to 17 mm and an equivalent thickness of 0.032 mm;
- Basalt grid B2 (Figure 3*b*): bidirectional balanced basalt grid characterized by a weight density of 400 g/m^2, a nominal bundle spacing equal to 8 mm and an equivalent thickness of 0.064 mm;
- Aramid-glass grid AG (Figure 3*c*): bidirectional unbalanced grid realized with aramid and alkali-resistant glass fibers, characterized by a weight density of 250 g/m^2, a nominal bundle spacing equal to 15 mm and equivalent thicknesses of 0.031 mm (warp) and 0.049 mm (weft);
- Steel fibers S1 (Figure 3*d*): unidirectional steel fiber strips, made of high-strength steel micro-cords, characterized by a weight density of 670 g/m^2, an effective area of the cords equal to 0.538 mm^2 and an equivalent thickness of 0.084 mm (0.157 cords/mm);
- Steel fibers S2 (Figure 3*e*): unidirectional steel fiber strips, made of high-strength steel micro-cords, characterized by a weight density of 1200 g/m^2, an effective area of the cords equal to 0.538 mm^2 and an equivalent thickness of 0.169 mm (0.314 cords/mm).

(a) (b) (c) (d) (e)

Figure 3. Grid and strip reinforcements: (a) B1; (b) B2; (c) AG; (d) S1; (e) S2.

The mechanical anchorages (Figure 4) consisted of helicoidal stainless steel bars, with a diameter of 10 mm, inserted into drilled through-holes and fixed, on both sides of the panels, by

polypropylene pins. The polypropylene pins are placed over the first mortar matrix layer and over the grid or strip reinforcements. They are then covered by the second mortar matrix layer.

(a) (b) (c) (d)

Figure 4. Mechanical anchorages: (a) helicoidal steel bars; (b) cutting of the grid; (c-d) polypropylene pin.

The adopted composite systems were subject to direct tensile tests and bond tests according to standard procedures, also adopted in previous researches [28,66]. Three samples for each test and for each strengthening system were built in the laboratory and tested after 28-40 days, coherently with the tests on the wall panels. More in detail, direct tensile tests were not performed on dry fibers but on FRCM/SRG coupons, having different dimensions according to the geometry of the grid reinforcements (Table 3). The failure mode was characterized, for all the strengthening systems, by the rupture of the fibers and by several cracks within the mortar matrix. The tensile stresses were evaluated considering the cross section of the dry fibers. The average results of the direct tensile tests are reported in Table 3, in terms of fiber tensile strength $f_{t,f}$, ultimate strain ε_u and elastic modulus E_f. In particular, the elastic modulus was determined from the final branch of the constitutive law, in which the mortar matrix was fully cracked [24,26].

Bond tests were performed according to standard single-lap shear test setup [30,67]. Details about the specimen dimensions are reported in Table 4: it is worth mentioning that the bond length was always greater than the effective bond length. The results of the bond tests are reported in Table 4 in terms of average bond strength $f_{b,f}$, evaluated considering the cross section of the dry fibers. The efficiency η of the grid or strip reinforcements, representing the ratio between the bond strength and the tensile strength, was also evaluated (Table 4). The highest values (> 85%) were associated with reinforcements failing, in the bond tests, due to the rupture of the fibers (B1 and AG), while the lowest values (< 70%) were observed for reinforcements showing a prevalent delamination at the matrix-

fiber interface (B2, S2). An intermediate efficiency value was registered for the S1 reinforcement, for which both failure modes took place during the bond tests. Tensile and bond tests on the grid reinforcements AG were performed on single-layer FRCM systems only.

It can be noticed that the thickness of some composite systems was slightly different in tensile and bond tests, and different to the one adopted in the application on the wall panels. It is worth mentioning that the experimental results of the tensile tests are function of the dry fibers only. Moreover, preliminary tests showed that the variation of the mortar matrix thickness, in the range of 2-4 mm, is irrelevant with respect to the bond strength and failure mode.

Table 3. Direct tensile tests on FRCM/SRG coupons: experimental results.

Strengthening system	Sample dimensions (mm^3)	$f_{t,f}$ (MPa)	C.o.V. (%)	ε_u (%)	C.o.V. (%)	E_f (GPa)	C.o.V. (%)
B1	400×40×10	1160	3.3	2.2	5.1	76.1	6.8
B2	400×40×10	963	6.1	1.1	7.3	66.2	12.1
AG	500×75×6	1467	11.4	1.2	8.4	115.0	9.3
S1	500×50×6	2857	7.9	1.7	4.2	200.9	5.8
S2	400×40×6	2867	5.8	2.1	10.5	186.6	12.1

Table 4. Bond tests: experimental results.

Strengthening system	Masonry prism (mm^3)	Bond length (mm)	Bond width (mm)	Thickness (mm)	$f_{b,f}$ (MPa)	C.o.V. (%)	η (%)
B1	120×120×445	345	50	8	1058	7.3	91.2
B2	120×120×445	345	50	8	616	5.8	63.9
AG	120×250×315	260	75	6	1275	9.2	86.9
S1	120×250×315	260	50	6	2245	11.7	78.6
S2	125×125×380	300	50	6	889	8.2	31.0

3.4 Diagonal compression test

Diagonal compression tests were carried out following the indications provided by the ASTM E519 and RILEM LUMB6 Standards [68,69], with the objective of analyzing the shear behavior of the investigated masonry samples. The panels were tested between 28 and 40 days from the application of the composite systems, in accordance with the tests on the materials. In order to properly capture both the pre-peak and the post-peak behaviour, tests were performed under displacement control. A servo-hydraulic actuator, having a maximum capacity of 500 kN, was used for the application of the diagonal compression displacement, with a rate equal to 0.01 mm/s. The

measurements of the diagonal shortenings or elongations were done by means of linear potentiometers, with 50 mm stroke and 1100 mm gage length, positioned on both sides of the masonry panels, along the two diagonals. The setup of the test is shown in Figure 5. Steel cradles allowed the specimens to be seated properly.

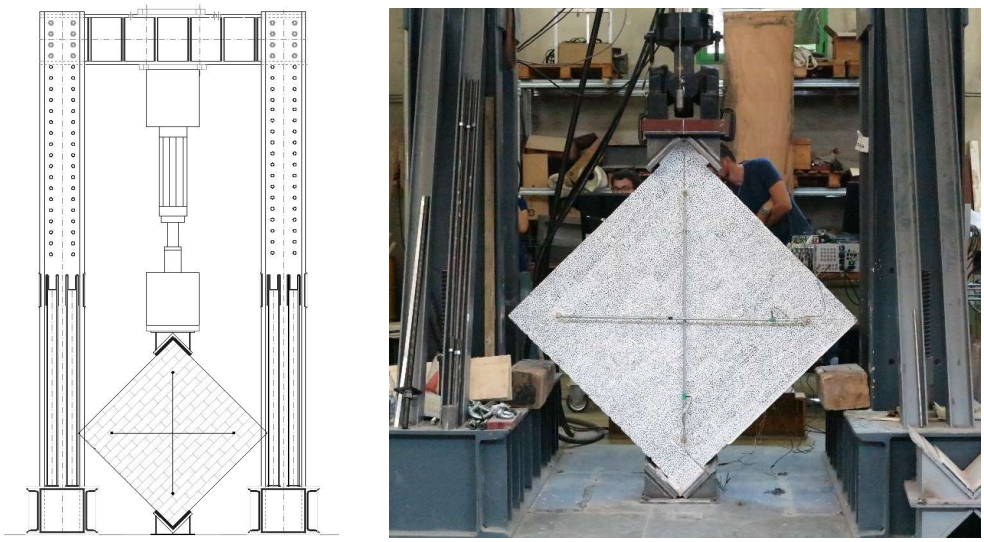

Figure 5. Diagonal compression test setup.

According to the theoretical interpretation of the diagonal compression test, based on an elastic solution of the problem [70–72], the stress state in the center of the wall panel can be calculated as:

$$\sigma = 0.56\frac{P}{A_n} \tag{5}$$

$$\tau = 1.05\frac{P}{A_n}, \tag{6}$$

where P is the applied diagonal load and A_n is the net cross section of the sample, evaluated as the product between the thickness and the average between the dimensions of the sample. In this configuration, the principal directions in the middle of the panel are aligned with the diagonals and the principal stresses at failure can be calculated as:

$$\sigma_I = f_{t,M} = 0.5\frac{P_u}{A_n} \tag{7}$$

$$\sigma_{II} = 1.62\frac{P_u}{A_n}, \tag{8}$$

where $f_{t,M}$ is the masonry diagonal tensile strength, and P_u is the panel failure load.

Since during the tests elongations and shortenings are measured along the two diagonals, the shear strain γ can be determined as:

$$\gamma = \varepsilon_c + \varepsilon_t \,, \tag{9}$$

where ε_c and ε_t are the compression and the tensile diagonal deformations, respectively, calculated as the average between the corresponding deformations on the two sides of the specimen.

Considering the experimental shear stress *vs* shear strain curve, the sample shear modulus *G* was here evaluated as the secant modulus between 1/10 and 1/3 of the failure load.

4 Experimental results

The analysis of the results presented in this Section allows to evaluate the influence of the investigated parameters, in terms of masonry quality, bond pattern and chosen composite system, on the shear behavior of the FRCM/SRG strengthened samples. With this purpose, comparisons between the results of the diagonal compression tests performed will be discussed.

Representative failure modes are reported in Figure 6 for an unreinforced sample (Figure 6*a*), a sample reinforced with a continuous FRCM strengthening system (Figure 6*b*), and two samples strengthened with the discontinuous SRG systems, considering both the adopted layouts (Figure 6*c,d*). All the unreinforced masonry specimens failed with a similar crack pattern, governed by the presence of a main crack along the compressed diagonal. On the other hand, thanks to the presence of the grid or strip reinforcements, multiple cracks were visible on the surfaces of the FRCM/SRG strengthened panels, aligned along the compressed diagonal and characterized by a lower opening with respect to the crack appeared on the unreinforced samples. By comparing the failure modes for the masonry panels strengthened by discontinuous layouts, it is worth noticing that the cracking process started from the unreinforced masonry substrate in the middle of the samples and then involved also the mortar matrix along the reinforcing strips. A more widespread cracking of both the masonry and the unidirectional reinforcement layers was visible for the panel strengthened with a higher number of strips (Figure 6*d*). In general, the presence of the considered mechanical anchorages

did not seem to strongly affect the crack patterns. Masonry crushing was not observed in the experimental tests. Concerning the failure mode of the FRCM systems, the delamination at the matrix-fiber interface was the predominant failure mode for all the samples, especially for grid reinforcement characterized by a high weight density. In few cases only (samples B-F_A_B1, B-F_A_B1-MA and B-H_A_B1-MA), besides the delamination, the tensile rupture of a limited number of bundles occurred at large displacements for compatibility reasons, in correspondence with macroscopic cracks in the mortar matrix.

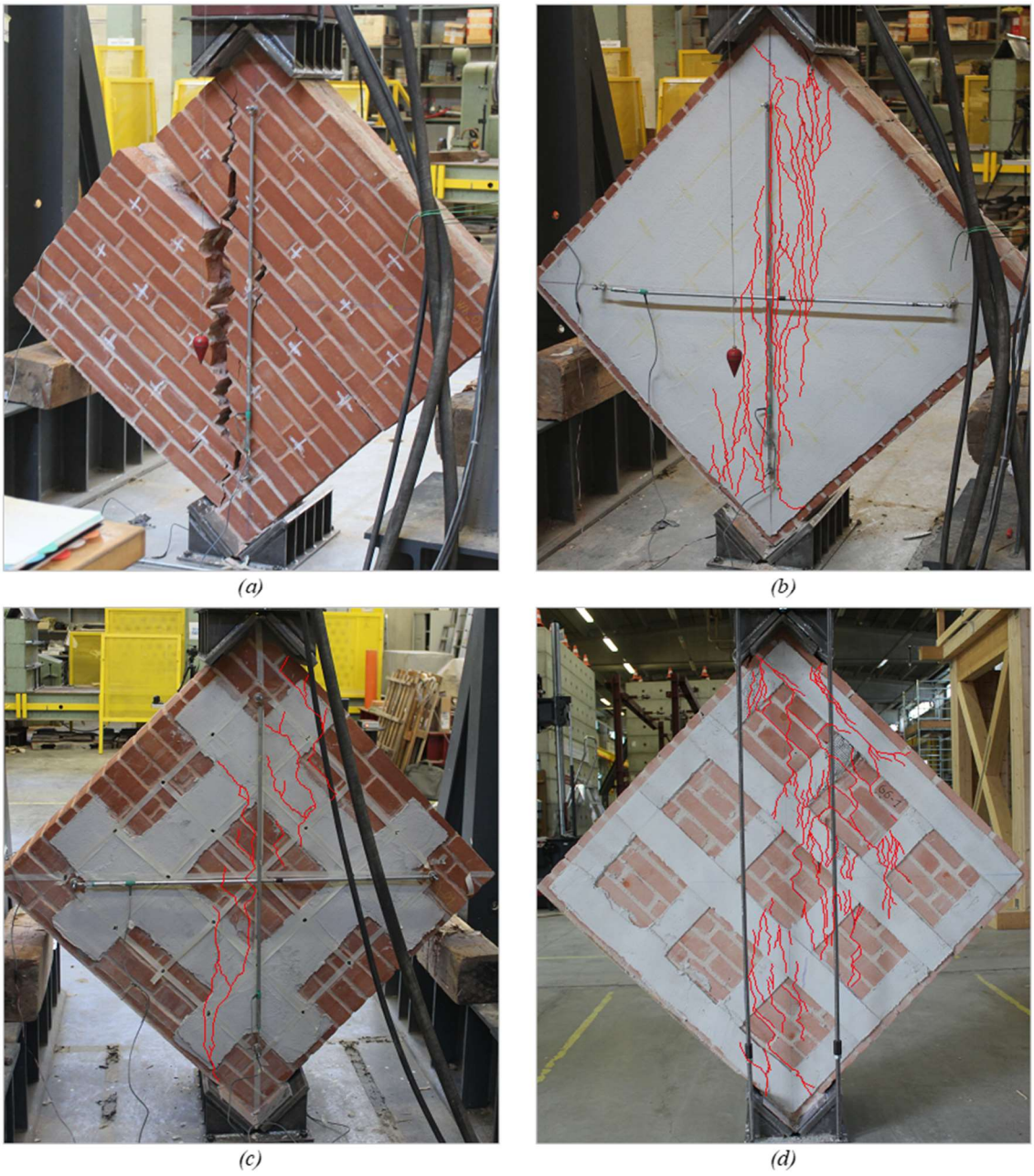

Figure 6. Representative failure modes: (a) B-FF_A_URM; (b) B-H_A_B1-MA; (c) B-F_A_S1-MA; (d) B-F_B_S1.

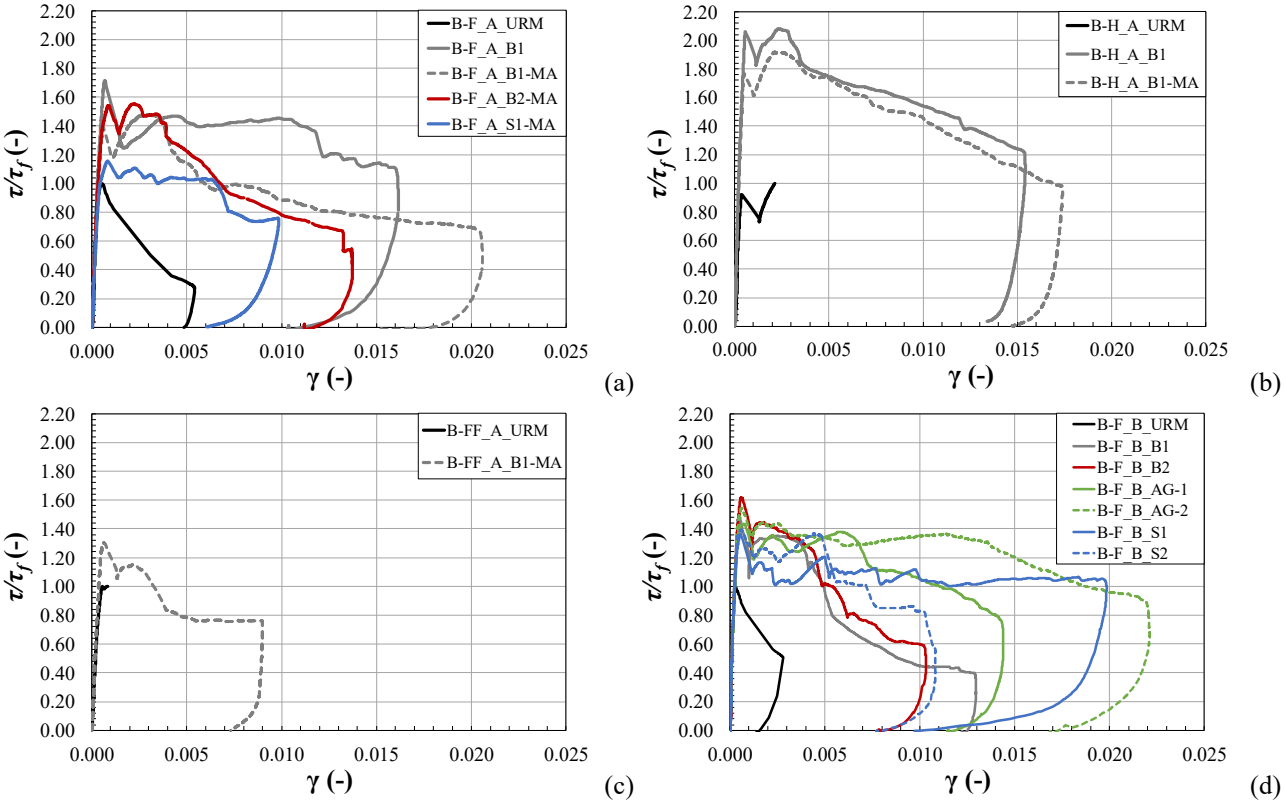

Figure 7. Shear stress *vs* shear strain diagrams: (a) B-F_A samples; (b) B-H_A samples; (c) B-FF_A samples; (d) B-F_B samples.

The shear stress *vs* shear strain diagrams are reported in Figure 7, distinguishing between the different masonry typologies and bond patterns considered. The diagrams are normalized with respect to the maximum shear stress registered for the URM sample of the corresponding masonry typology. The unreinforced masonry panels, after an almost linear elastic branch until the peak load, were characterized by a brittle or quasi-brittle failure mode, as expected. The curves of the FRCM/SRG strengthened samples generally showed an initial branch which can be considered linear elastic up to the first peak, significantly higher than the peak stress of the corresponding URM samples. In few cases, a stiffness degradation was visible in the ascending branch, approaching the peak load. Subsequently, a drop in the load bearing capacity was registered, followed by a second or multiple peaks, depending on the adopted strengthening technique, as will be thoroughly described in Section 5. For all the samples, the first peak load corresponded to the appearance of the first macroscopic cracks, i.e. in the mortar matrix for panels strengthened with a continuous layout or in the central masonry portion for panels strengthened with a discontinuous layout. In the post-peak phase, the

mortar matrix progressively cracked, and the role of the fibers became more important, influencing the failure mode and the deformation capacity of the FRCM/SRG strengthened samples.

The post-peak behavior of the samples strengthened by continuous FRCM systems was usually characterized by a second peak load followed by a softening behavior until final failure, considered in correspondence of a widespread state of damage or at detachment of reinforcement portions. In the majority of the cases, the second peak was lower than the first one, with the exception of few panels of the masonry typology *A* strengthened by bidirectional basalt grids, for which the second peak load was the maximum load registered. This behavior could indicate a greater efficiency of the grid reinforcements, able to further improve the shear capacity of the samples after the cracking of the mortar matrix and it was probably related, for some samples (B-F_A_B1-MA, B-F_A_B2-MA, B-H_A_B1-MA), to the presence of the mechanical anchorages, which allowed the grid reinforcements to better carry the tensile stresses, improving the bond between the FRCM and the masonry.

For the discontinuous SRG systems, the first peak, as already mentioned, was related to the first cracking of the masonry panel in the central portion of the samples, not reinforced. Then, the presence of multiple peaks was registered, corresponding to the progressive cracking of the SRG strips crossing the compressed diagonal. The corresponding shear stress *vs* strain diagrams (Figure 7*a,d*) show that the discontinuous layout adopted for the masonry typology *B* (Figure 2*c*) was the most efficient, due to the reduced spacing between the unidirectional strips, resulting in a smaller unstrengthened portion in the center of the sample.

The results of the diagonal compression tests are summarized in Table 5, where the first peak load P_1, the second peak load P_2 and the maximum capacity P_u of the panels are reported, together with the strength increment calculated as the ratio between the failure load P_u and the failure load of the corresponding unreinforced (URM) sample. The maximum shear stress τ_u and the masonry tensile strength $f_{t,M}$, evaluated through Equations (6) and (7) are presented as well. In addition, the shear strains γ_1 and γ_2 in correspondence with P_1 and P_2, respectively, and the shear modulus G are reported.

Table 5. Diagonal compression test results.

Sample code	P_1 (kN)	P_2 (kN)	P_u (kN)	$P_u/P_{u,URM}$ (-)	τ_u (MPa)	$f_{t,M}$ (MPa)	γ_1 ($\times 10^{-3}$)	γ_2 ($\times 10^{-3}$)	G (MPa)	μ (-)
B-F_A_URM	206.1	-	206.1	-	0.79	0.37	0.54	-	2660	4.0
B-F_A_B1	351.7	301.1	351.7	1.71	1.35	0.64	0.69	4.39	2769	24.9
B-F_A_B1-MA	284.3	303.7	303.7	1.47	1.16	0.55	0.61	3.13	2649	13.9
B-F_A_B2-MA	316.1	318.7	318.7	1.55	1.22	0.58	0.88	2.25	2810	10.9
B-F_A_S1-MA	237.3	227.8	237.3	1.15	0.91	0.43	0.83	2.26	2648	18.4
B-H_A_URM	136.2	-	154.3	-	0.56	0.27	0.38	-	1889	-
B-H_A_B1	319.3	322.8	322.8	2.09	1.17	0.56	0.56	2.37	2601	18.5
B-H_A_B1-MA	273.8	296.8	296.8	1.92	1.07	0.51	0.50	2.13	2538	29.9
B-FF_A_URM	221.2	-	221.2	-	0.85	0.40	0.82	-	2277	-
B-FF_A_B1-MA	288.1	254.5	288.1	1.30	1.10	0.53	0.65	2.25	2994	7.9
B-F_B_URM	183.7	-	183.7	-	0.64	0.30	0.30	-	3056	4.4
B-F_B_B1	276.7	248.6	276.7	1.51	0.96	0.46	0.47	2.54	3216	13.3
B-F_B_B2	295.8	264.4	295.8	1.61	1.04	0.49	0.61	1.78	2705	10.9
B-F_B_AG-1	262.4	247.7	262.4	1.43	0.92	0.44	0.74	2.25	2868	7.5
B-F_B_AG-2	282.9	265.2	282.9	1.54	0.99	0.47	0.61	1.76	2436	19.0
B-F_B_S1	251.2	214.6	251.2	1.37	0.87	0.42	0.56	1.54	2933	23.3
B-F_B_S2	254.7	231.1	254.7	1.39	0.89	0.42	0.58	1.89	3171	42.4

By comparing the results of the unreinforced samples for the masonry typology *A* it is noticeable that the lowest shear capacity was registered for the masonry panel characterized by the header bond pattern (B-H_A_URM). Indeed, due to the low height-to-width ratio of the bricks within the masonry texture, the development of a preferential crack path, involving only mortar joints along the compressed diagonal, was observed. The two samples characterized by the Flemish (B-F_A_URM) and the false Flemish bond (B-FF_A_URM), instead, reached a similar value of the failure load, indicating that the transverse connection between the wall leaves for the sample B-FF_A_URM was probably guaranteed by the presence of the mortar only. As expected, the shear capacity of the unreinforced sample for the masonry typology *B* (B-F_B_URM) was lower than that of the corresponding sample of the masonry typology *A* (B-F_A_URM), given the differences in the mortar quality between the two investigated masonry typologies.

A significant strength increment was observed for the FRCM/SRG strengthened samples with respect to the unreinforced ones, highlighting the crucial role of the composite systems in enhancing

the shear capacity of masonry panels. With the objective of comparing the efficiency of the different composite systems, the average strength increments are reported in Table 6 together with the strength per unit length that each composite system can nominally provide. The latter was calculated as the fiber conventional stress limit [53], taken as the minimum between the tensile strength $f_{t,f}$ and the bond strength $f_{b,f}$, multiplied by the fiber equivalent thickness (for continuous strengthening systems) or by the ratio between the width of the SRG strip and the strip spacing (for discontinuous strengthening systems). It can be observed that continuous FRCM strengthening systems with single-layer configuration are the most efficient ones. It is also worth mentioning that the average strength increments for all the continuous FRCM systems, including the double-layer configuration, are similar between each other, suggesting that the registered increment could not depend on the amount and on the strength of the fiber only, as will be discussed in the following. Discontinuous SRG strengthening systems are the less effective, providing a limited strength increment in comparison with the strength per unit length, which is higher than the others. This is certainly related to the fact that these systems do not cover the central portion of the masonry panels, which is subject to the highest tensile stresses during the diagonal compression test, especially at the onset of cracking.

Table 6. Comparison between the efficiency of the different FRCM/SRG strengthening systems.

Strengthening system	Average strength increment P_u / $P_{u,URM}$ (-)	Strength per unit length (N/mm)
B1 Reinforcement	1.67	33.9
B2 Reinforcement	1.58	39.4
AG Reinforcement (single-layer)	1.43	39.5
AG Reinforcement (double-layer)	1.54	79
S1 Reinforcement	1.26	56.6
S2 Reinforcement	1.39	42.9

The presence of the composite reinforcements, spreading the stresses over a larger portion of the samples, levels out the capacity differences between masonry panels characterized by diverse textures: the critical issues related to the preferential crack path observed for the unreinforced

specimen characterized by the header bond (B-H_A_URM) disappeared, and the strengthened masonry panels of the series B-H_A provided for two of the highest shear capacities. Moreover, similar first peak loads were registered for all the samples of the masonry typology *A* strengthened with bidirectional basalt grids, showing a very limited dependence of the capacity of the strengthened samples on the masonry texture adopted.

The analysis of the experimental behaviors showed that the failure of the strengthening systems (delamination or rupture) was never observed at first peak but it developed later, in correspondence of higher strain values. On the contrary, the first peak was always governed by the tensile failure of the mortar matrix, coherently with the observed crack development. As a confirmation, a trend can be recognized, at least considering the masonry panels strengthened with continuous FRCM systems: samples reinforced with the same mortar matrix, i.e. same type and same total thickness, reached similar peak load values P_1, which represented the shear capacity in most of the tests. Therefore, it can be stated that the expected strength increment associated to the mortar matrix is related to the increase of the uncracked resistance of the masonry panels. This aspect has been further developed in the following through a predictive analytical approach.

In terms of shear stiffness, the presence of the composite systems does not clearly produce significant increments, except for some samples of the masonry typology *A*, whose corresponding unreinforced sample was characterized by a rather low value of the shear modulus *G*. In general, similar values of the shear stiffness were found for the strengthened samples and these values were in line with the ones evaluated for unreinforced masonry panels, confirming the suitability of these materials in improving the shear behavior without determining considerable variations in the stiffness distribution among the structural components of existing buildings. In general, it can be stated that the increment in terms of shear stiffness given by the composite systems can be limited or negligible if the thickness of the strengthening system is much lower than the wall thickness and if the reinforced masonry panels are characterized by a good-quality masonry typology. It is also worth noticing that the slope of the reloading branch, after first cracking, up to the second peak load can be related to the

axial stiffness of the grid reinforcements: typically, along this branch, higher values of axial stiffness are associated with higher slopes of the shear stress *vs* shear strain curve. Despite the variability of the slopes of the reloading branches among the different strengthened masonry panels, the described trend can be recognized by considering the shear strain increase $\Delta\gamma$ plotted against the axial stiffness $E_f A_f$, for the continuous FRCM systems (Figure 8): as expected, the higher the axial stiffness, the lower $\Delta\gamma$.

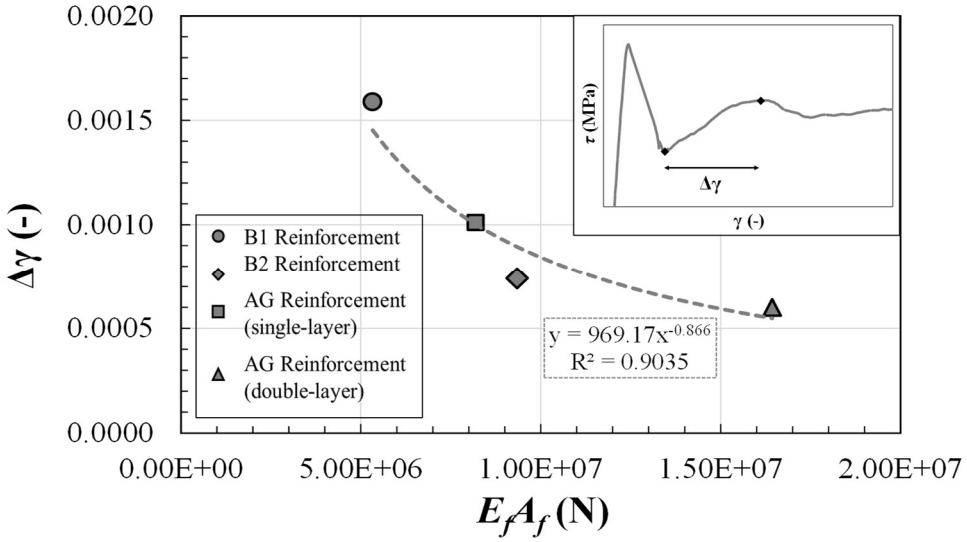

Figure 8. Shear slip increment *vs* axial stiffness of the continuous reinforcements.

The pseudo-ductility μ (Table 5), assuming a simplified elastic-perfectly plastic behavior of the samples, was determined as the ratio between the ultimate shear strain γ_u, taken in correspondence with a 20% drop in the load bearing capacity after the peak, and the shear strain γ_y, identified along the initial linearized branch in correspondence with a load value equal to 0.8 P_u. μ was evaluated to better analyze the role of the strengthening systems in improving the failure mode of the masonry structural elements, which passed from a quasi-brittle failure mode to a more ductile one. To properly consider the role of the fibers, which is prevalent after the cracking of the mortar matrix, the ultimate shear strain γ_u was not taken along the descending branch after the first peak load, but after the subsequent peak (if present).

The values of the pseudo-ductility factor μ clearly demonstrate that the presence of the strengthening systems can significantly reduce the brittleness of the shear failure for masonry panels.

Indeed, in most of the cases, quite high values were attained, for both the masonry typologies. A pseudo-ductility factor equal to at least twice the factor evaluated for unreinforced samples was obtained, even if, by comparing the performance of different composite systems in terms of ductility, a clear trend cannot be established.

5 Interpretation of experimental results

Based on the analytical formulations presented in Section 2, to precisely assess the efficiency of the strengthening systems in improving the shear capacity of masonry panels, the strength increments should be compared with the expected fiber contribution $V_{t,f}$, accounting for both the amount of the reinforcing fibers and their ultimate strength. In terms of strength, given the results of the mechanical characterization of the composite systems (Table 3 and Table 4), the bond strength would represent the governing parameter, as confirmed by the experimental evidences. Indeed, during the diagonal compression tests, the composite systems mainly failed due to delamination phenomena and rarely due to some local tensile rupture of the fibers. The comparison between the experimental strength increment and the analytical one ($V_{t,f}$) implies that the failure of the FRCM/SRG reinforcements takes place in correspondence with the reaching of the maximum load P_u. However, this condition is not coherent with the experimental outcomes, since, in the majority of the cases, P_u coincided with the first peak load, not associable to the failure of the fibers.

The experimental results, indeed, clarified the crucial role of the mortar matrix in the definition of the first peak load of the strengthened masonry panels, when a macroscopic cracking of the matrix itself developed along the compressed diagonal (see Section 4). In many cases, this first peak corresponded also to the shear strength. For this reason, the role of the fibers is expected to mainly influence the post-first peak behavior, since they started working (alone and effectively) after the cracking of the matrix, carrying the tensile stresses and distributing them over the whole surface of the samples. Similar conclusions were found with regards to the behavior of masonry panels

strengthened by CRM systems [57,59,60], whose shear capacity was related to the presence of a thick mortar matrix layer, rather than to the presence of the composite grid.

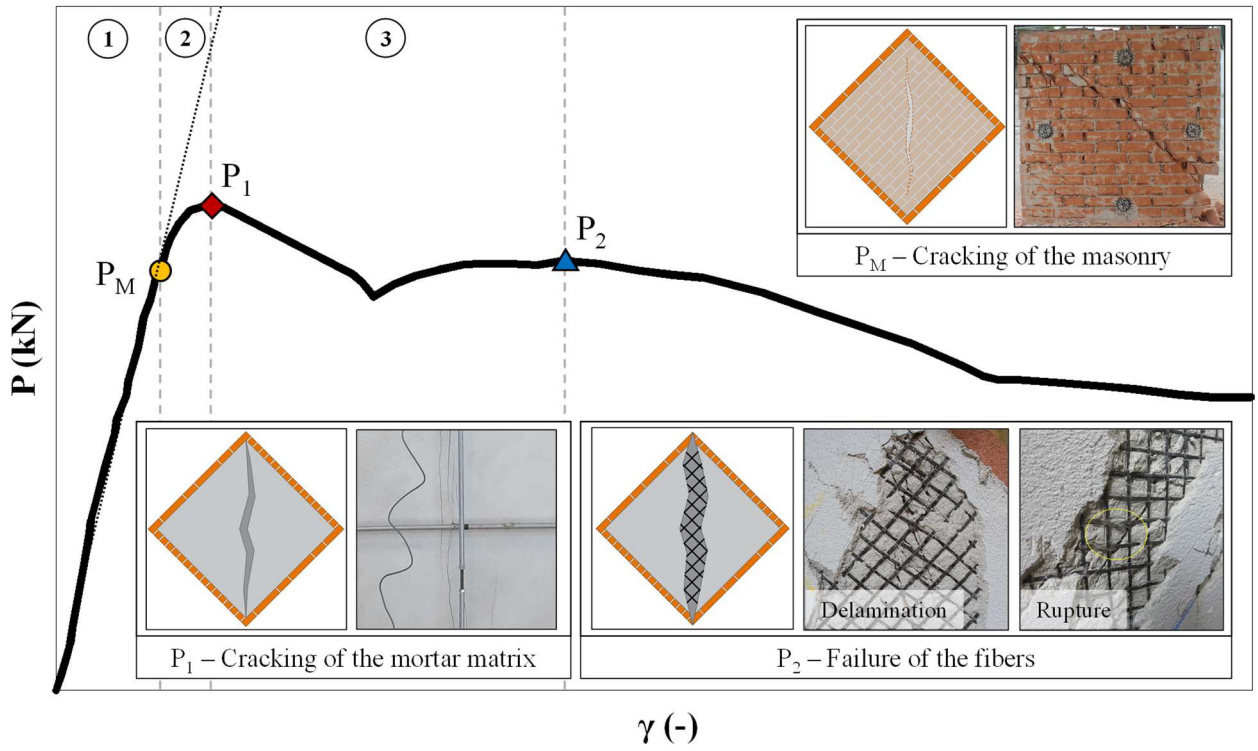

Figure 9. Diagonal force *vs* shear strain behavior of a strengthened panel in a diagonal compression test.

From the mechanical point of view, the shear behavior of a FRCM/SRG strengthened masonry panel during a diagonal compression test can ideally be subdivided into three different phases, whose force *P vs* shear strain γ curve is reported in Figure 9: (1) the masonry substrate and the composite system (matrix and fibers homogenized) work together, until the onset of cracking of the masonry substrate, recognizable by the change in the slope of the curve (point P_M in Figure 9); (2) the composite system (matrix and fibers homogenized) works alone across the masonry cracks, with a perfect bond between mortar matrix and fibers, up to the onset of cracking of the matrix (point P_1 in Figure 9); (3) only the fiber grid or strip is working across diagonal cracks until fibers failure (point P_2 in Figure 9). It is worth mentioning that these phases were recognized from the experimental results, even if, for some strengthening layouts, only one panel was tested. Through the comparison of the diagonal compression test results performed on all the samples, together with the complete

mechanical characterization of the materials, it was possible to reliably interpret the described shear behavior, even if more tests could be useful for a more precise quantitative definition.

To better analyze the composite system contribution in a masonry diagonal compression test, its shear stress τ *vs* shear strain γ diagram can be derived as the difference between the diagrams registered for the strengthened panel and for the corresponding URM sample [60], under the reasonable assumption of considering the behavior of the URM sample as representative of the behavior of the masonry substrate in the strengthened panel. More specifically, for any given value of γ, the τ related to the composite system was obtained as the difference between the shear stresses coming from the strengthened and unstrengthened curves. Figure 10 shows the experimental curves for one panel strengthened by the basalt B1 reinforcement and the corresponding URM panel, together with the FRCM curve obtained as just described. In the strengthened curve, the three previously identified phases and key points are indicated. According to the proposed approach, it can be noticed that the contribution of the composite system is limited in the initial part of the test (phase 1*a* in Figure 10), while it becomes significant during the cracking process of the masonry substrate, which corresponds to the stiffness degradation visible in the curve of the URM sample and to the slope increase in the curve of the composite system (phase 1*b* and shaded area in Figure 10). After the complete plain masonry diagonal cracking (when the URM sample reaches its maximum capacity), the composite system works alone up to the first peak of the curve (phase 2 in Figure 10) and the slope of the curve further increases. The behavior of the composite system during these phases (1*b* and 2) is bi-linear, with a slight stiffness increase in correspondence with the maximum load sustained by the URM sample. The first peak in the composite system diagram (matrix cracking) is followed by a drop in the load bearing capacity (due to cracks opening) and by a subsequent force increment, related to the presence of the basalt grid becoming fully effective. The force increases up to a second peak load, corresponding to the beginning of the fiber's failure or their delamination from the matrix. The whole process of matrix cracking and fiber activity until failure is named as phase 3.

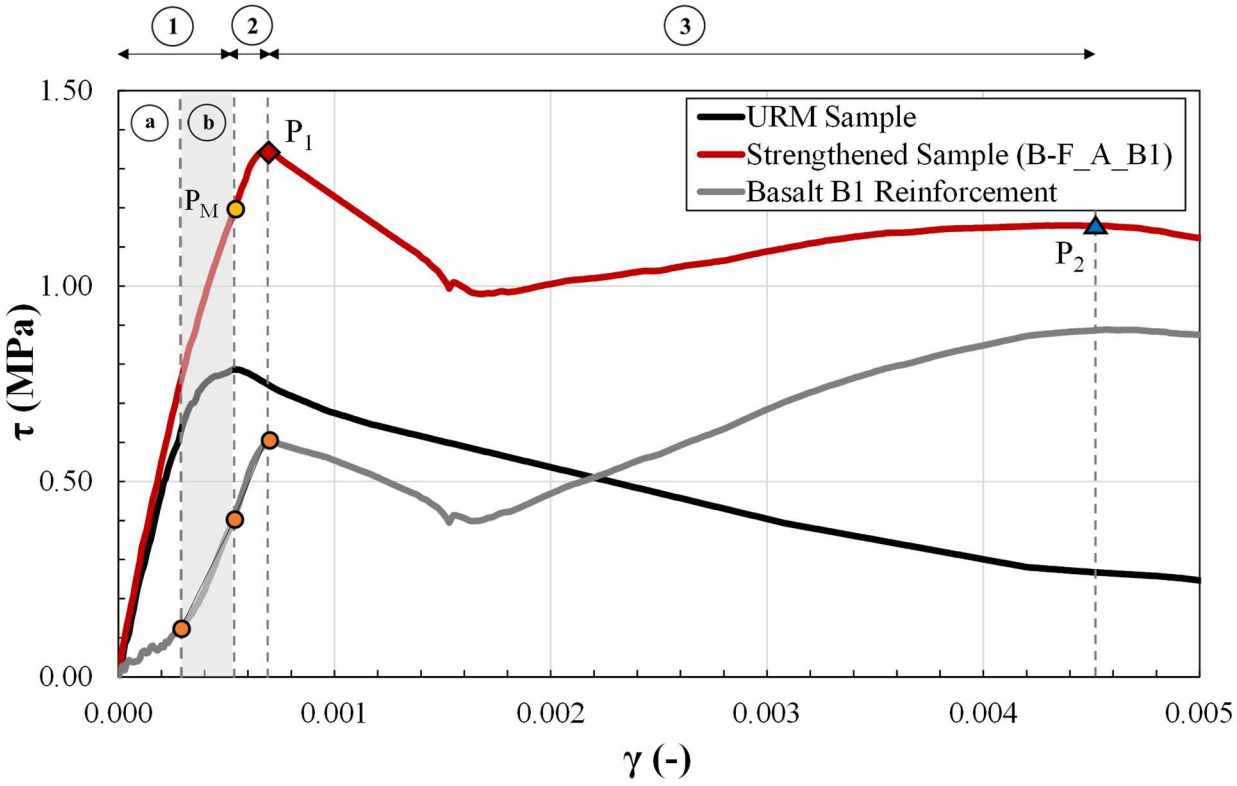

Figure 10. Shear stress *vs* shear strain diagrams: uncoupled behavior of the URM and FRCM contributions.

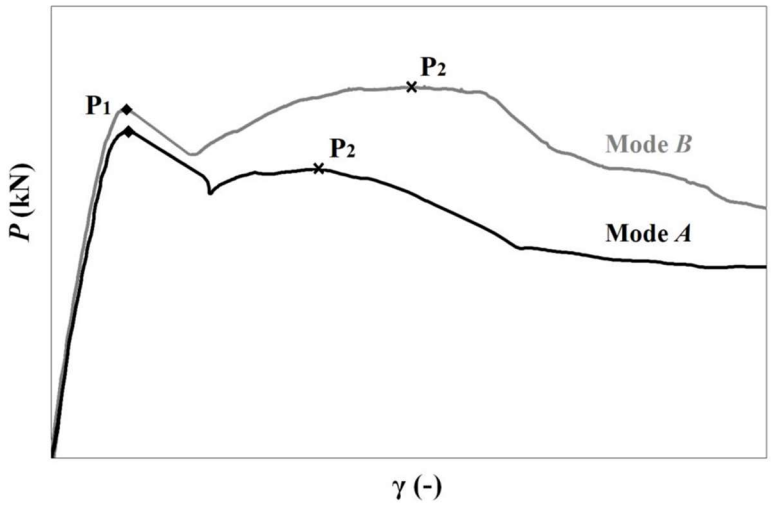

Figure 11. Typical shear behavior of masonry panels in a diagonal compression test.

Depending on the strength increment after matrix cracking, associated to the type and amount of reinforcement and to the softening behavior of the masonry substrate, the second peak load of the strengthened samples can result lower ($P_2 < P_1$, mode *A* in Figure 11) or higher ($P_2 > P_1$, mode *B* in Figure 11) than the first peak load. The predominant condition was mode *A* among the tests carried out (9 samples out of 13). Irrespective of the ratio between P_1 and P_2, the FRCM system curve (e.g. Basalt B1 reinforcement in Figure 10) presented in all cases a second peak higher than the first one,

which means that the fibers contribution alone was larger than that of the mortar matrix. This could not happen if a too small amount of fibers would be used or if their bond capacity would be really weak.

6 Analytical prediction of the shear capacity of FRCM strengthened masonry

According to the experimental observations and the previous remarks (Figure 9), it can be stated that P_1 is the load corresponding to the cracking of the matrix, while P_2 is the load associated with the failure of the fibers (rupture or delamination at the matrix-fiber interface).

In spite of the influence of the mortar matrix on the shear capacity of a FRCM/SRG strengthened panel, evidenced by the experimental outcomes, the mortar matrix contribution is not taken into account by the analytical formulations reported in Section 2, in which the composite system contribution is evaluated considering the presence of the fibers only. Therefore, in order to predict the shear strength of strengthened samples, an alternative analytical approach is here proposed. It is applicable for a variety of FRCM and SRG systems, but it is described in the following for continuous and symmetric strengthening layouts. In this framework, both the peak loads P_1 and P_2 should be evaluated; in fact, it is not known in advance which will be the bigger.

The load which leads to the first cracking of the mortar matrix (P_1) can be evaluated as:

$$P_1 = P_M + P_{mx}, \tag{10}$$

where P_M is the plain masonry contribution and P_{mx} is the mortar matrix contribution. They can be determined by considering the tensile strength of the two components (masonry and matrix), as if they were separately subject to a diagonal compression test but both reaching their maximum capacity at the same moment. As recalled earlier (Figure 10), this is not rigorously true: masonry cracking is believed to happen before matrix cracking and the quasi-brittle behavior of masonry (softening) should be taken into account after its cracking. However, the error introduced by the approximation in Equation (10) seems acceptable, also considering all the uncertainties involved in the prediction process. In addition, the introduced simplification allows to evaluate the two terms in Equation (10)

by using a limited number of parameters, increasing the overall robustness of the approach. In particular, the contributions can be evaluated by considering the inverse formula of Equation (7) as:

$$P_M = \frac{f_{t,M} \cdot A_n}{0.5}, \tag{11}$$

$$P_{mx} = \frac{f_{fl,m} \cdot A_{mx}}{0.5}, \tag{12}$$

where $f_{t,M}$ is the masonry tensile strength and $f_{fl,mx}$ is the mortar matrix flexural strength. The former can be derived from diagonal compression tests performed on unreinforced masonry, while the latter can be evaluated by standard laboratory tests [65]. A_n is the net cross section of the masonry panel and A_{mx} is the net cross section of the mortar matrix, evaluated as the total thickness of the matrix layers, on both sides of the panel, multiplied by the width of the strengthened area. To be mentioned the fact that the contribution of the fiber is not taken into account since it can be considered negligible at this stage (average capacity increment less than 3%). Moreover, the influence of the self-weight of the masonry panel can be disregarded since it represents a minimum percentage of the failure load, as confirmed by the experimental results.

The proposed formulation, already adopted for the evaluation of the shear strength of CRM strengthened panels [57,59,60] is here extended to the case of FRCM strengthened samples. It seems consistent with the assumption of an elastic behavior of the reinforced samples up to the cracking of the matrix and of a perfect bond between the composite system and the masonry substrate. The difference with the formulation proposed for CRM systems is related to the use of the flexural strength of the mortar matrix ($f_{fl,m}$) instead of the tensile one ($f_{t,m}$) in Equation (12). The choice of using the flexural strength instead of the tensile strength is related to the fact that the stress distribution is not uniform over the cross section of the mortar matrix in a diagonal compression test. The crack involves the central portion first and then propagates vertically towards less stressed zones. Therefore, the use of the flexural strength is not related to the occurrence of some flexural phenomena but to the fact

that the attainment of the tensile capacity of the mortar matrix takes place progressively along the height of the wall panels.

Equation (10) was validated by comparing the predicted capacities with the experimental results (first peaks), reported in Table 7, obtaining a good agreement with an average absolute error of 6.7% (Figure 12). In particular, the evaluation of the predicted load $P_{1,th}$ was carried out by considering the masonry tensile strength $f_{t,M}$ experimentally obtained for the different tested masonry typologies (Table 5). For the masonry typology *A*, given the similar failure mode and ultimate loads of the unreinforced samples B-F_A_URM and B-FF_A_URM, the average tensile strength obtained from the two URM samples was adopted in the calculations.

Table 7. Shear strength prediction for FRCM strengthened panels: validation of the analytical approach.

Sample code	$P_{1,exp.}$ (kN)	P_M (kN)	P_{mx} (kN)	$P_{1,th.}$ (kN)	Error* P_1 (%)	$P_{2,exp.}$ (kN)	P_f (kN)	$P_{2,th.}$ (kN)	Error* P_2 (%)
B-F_A_B1	351.7	212.9	74.0	286.9	-18.4	301.1	202.1	282.1	-6.3
B-F_A_B1-MA	284.3	212.9	74.0	286.9	+0.9	303.7	202.1	282.1	-7.1
B-F_A_B2-MA	316.1	212.9	74.0	286.9	-9.3	318.7	235.3	292.4	-8.2
B-H_A_B1	319.3	225.5	78.5	304.0	-4.8	322.8	214.5	299.3	-7.3
B-H_A_B1-MA	273.8	225.5	78.5	304.0	+11.0	296.8	214.5	299.3	+0.8
B-FF_A_B1-MA	288.1	213.4	74.1	287.5	-0.2	254.5	202.5	282.7	+11.1
B-F_B_B1	276.7	184.1	94.7	278.8	+0.8	248.6	221.7	289.4	+16.4
B-F_B_B2	295.8	183.0	94.1	277.1	-6.3	264.4	256.5	295.1	+11.6
B-F_B_AG-1	262.4	183.0	94.1	277.1	+5.6	247.7	257.1	295.6	+19.3
B-F_B_AG-2	282.9	183.3	125.8	309.1	+9.2	265.2	-	-	-

* The "+" and "-" signs indicate overestimation or underestimation of the experimental results, respectively.

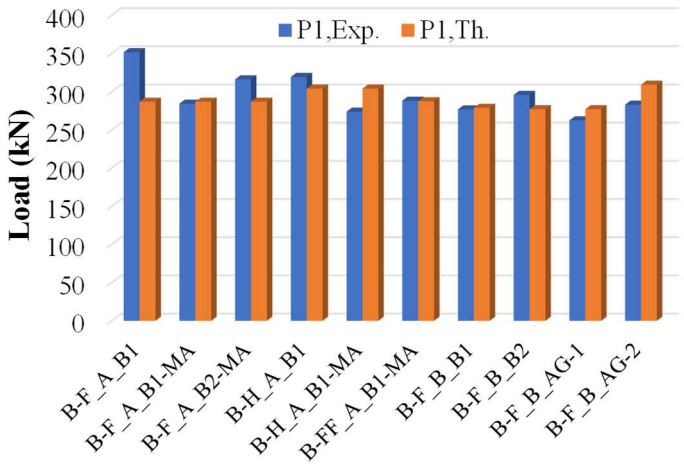

Figure 12. Experimental results *vs* analytical predictions for the evaluation of the first peak load.

After matrix cracking, the load corresponding to the failure of the grid reinforcement (P_2) can be evaluated as:

$$P_2 = \alpha_1 P_M + \alpha_2 P_{mx} + \alpha_3 P_f \,, \tag{13}$$

where the coefficients $\alpha_{i=1,3}$ are compatibility factors ($0 \leq \alpha_i \leq 1$), taking into account that the different constituents, after the first peak and across the main crack, can have different deformations and softening behaviors; P_M and P_{mx} correspond to the masonry and matrix contributions, already introduced, and P_f is the maximum diagonal load sustainable by the composite fibers alone, which can be determined as:

$$P_f = 2 f_f A_f \sqrt{2} \,, \tag{14}$$

where f_f is the fiber conventional stress limit [53], taken as the minimum between the tensile strength $f_{t,f}$ and the bond strength $f_{b,f}$, A_f is the cross section of the fibers in one direction, on both sides of the panel, and the term $\sqrt{2}$ is introduced to account for the inclination of the fibers with respect to the direction of the principal tensile stress (Figure 13) [58].

The determination of the load P_f (Equation 14) was carried out by considering the indications reported in Eurocode 2 [73] concerning the design of reinforced concrete structural elements with strut and tie models. Indeed, after the development of the cracking process, the continuum models used for the determination of the masonry and matrix contributions are no longer applicable to describe the resisting mechanism of the strengthened masonry panel. Therefore, it is here proposed the use of a strut and tie model, only based on equilibrium conditions. More in detail, according to Equation 6.59 of Eurocode 2 [73], referred to full discontinuity regions, the tensile force T of one of the two horizontal ties created inside the wall (and constituted by the grid reinforcement) can be expressed as a function of the diagonal load P according to the expression:

$$T = \frac{1}{4}\left(1 - 0.7\frac{a}{h}\right)P, \tag{15}$$

where h is the diagonal length of the panel and a is the width of the loaded area, here considered equal to 0 since the diagonal load can be assumed, for simplicity, as a pointwise force. With the aim of obtaining the maximum value of the diagonal load carried by the fibers alone ($P=P_f$), it is necessary to consider the maximum force T_f developed by the grid reinforcement at failure, which can be expressed as:

$$T_f = P_{f,s} \cos 45° = A_f f_f \frac{\sqrt{2}}{2}, \tag{16}$$

where $P_{f,s}$ is the maximum load that the bundles can take, which has to be projected along the horizontal direction (which is the direction of the tensile force T). For the calculation of T_f, half of the fibers crossing the mid-section of the wall panel (in both direction) were considered, since along the entire height of the wall there are two horizontal ties: this is the reason why the term A_f is included in the formulation. Equation 14 can then be easily obtained by inverting Equation 15 and introducing inside it the expression of T_f reported in Equation 16.

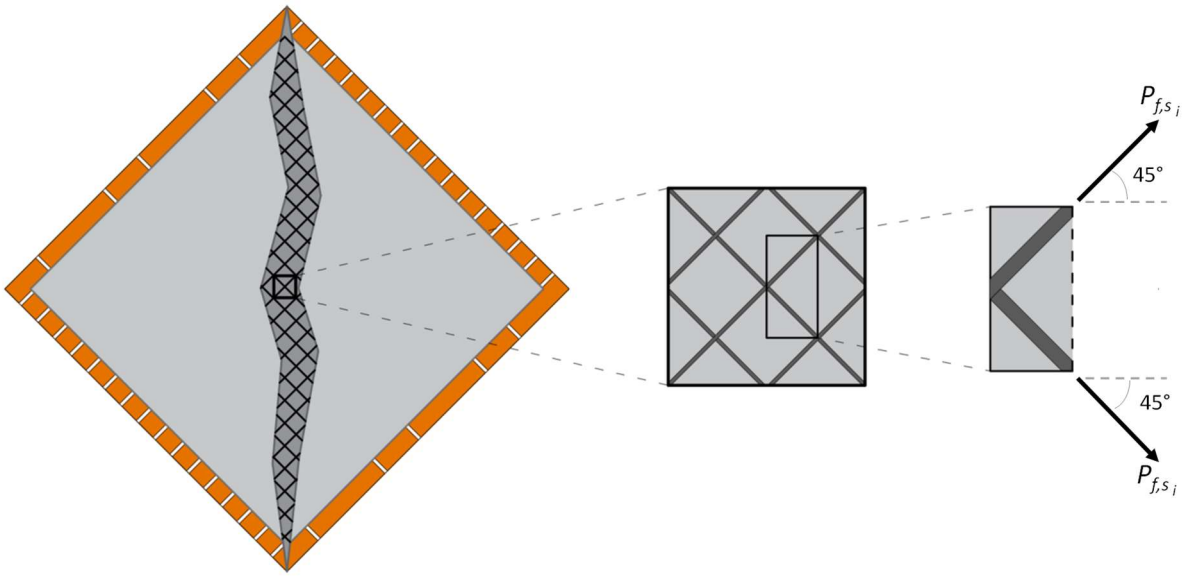

Figure 13. Orientation of the fibers with respect to the horizontal direction.

The coefficients α_1 and α_2 consider that after the first peak, the masonry and the matrix will soften, since they are quasi-brittle materials. In fact, P_2 always corresponds to a peak with a shear deformation larger than that of the first peak. The coefficient α_3, instead, is introduced to represent a reduced efficiency of the fibers in the investigated configuration. More in detail, values lower than

one are generally expected for this coefficient, mainly due to two aspects: (i) the direction of the principal tensile stresses is not coincident with the fibers alignment (Figure 13), therefore they are not subject to pure traction, and (ii) the fibers are not equally stressed along the main crack surface, since shear force produces a variable stress distribution, with the maximum values in the center of the samples.

With the aim of providing general indications for the determination of the factors α_i in practical applications, it should be noticed that they can be sensitive to the investigated masonry typology and the adopted strengthening system. More specifically, values of the coefficients α_1 and α_2, depending mainly on the brittleness of the masonry substrate and of the matrix, could vary according to the main crack opening, which is governed by the axial stiffness of the composite fibers ($E_f A_f$) and by their bond capacity: the stiffer the fibers, the higher the coefficients. As previously discussed, the slope of the reloading branch after the first peak of the shear stress *vs* shear strain curve is directly related to the stiffness of the composite fibers (Figure 8).

The three coefficients were calibrated by considering the experimental results relative to the second peak load P_2 (Table 5), as follows:

- The coefficient α_1 was directly evaluated as the ratio between the residual capacity of the URM samples, in correspondence with the second peak of the strengthened specimens, and the maximum capacity of the URM samples, further reduced by 20%. This reduction is considered to take into account the uncertainties in the softening curve of the URM panels. Moreover, in a strengthened panel, the masonry substrate is subject to a greater energy release, with respect to the URM panel at equal shear strain, when the failure of the fibers occurs. Therefore, the brittleness of the masonry substrate itself could be emphasized when composite systems are adopted.
- The coefficient α_2, due to lack of specific data or information, was calibrated by considering that the mortar matrix is characterized by a more brittle behavior with respect to the masonry

substrate, where dissipation can take place also due to the friction between constituents; for this reason, the coefficient α_2 was taken as the 20% of the coefficient α_1, meaning that the matrix contribution is almost negligible for P_2.

- The coefficient α_3 was indirectly evaluated by reversing Equation (13), inside which, at this stage, it was the only unknown parameter.

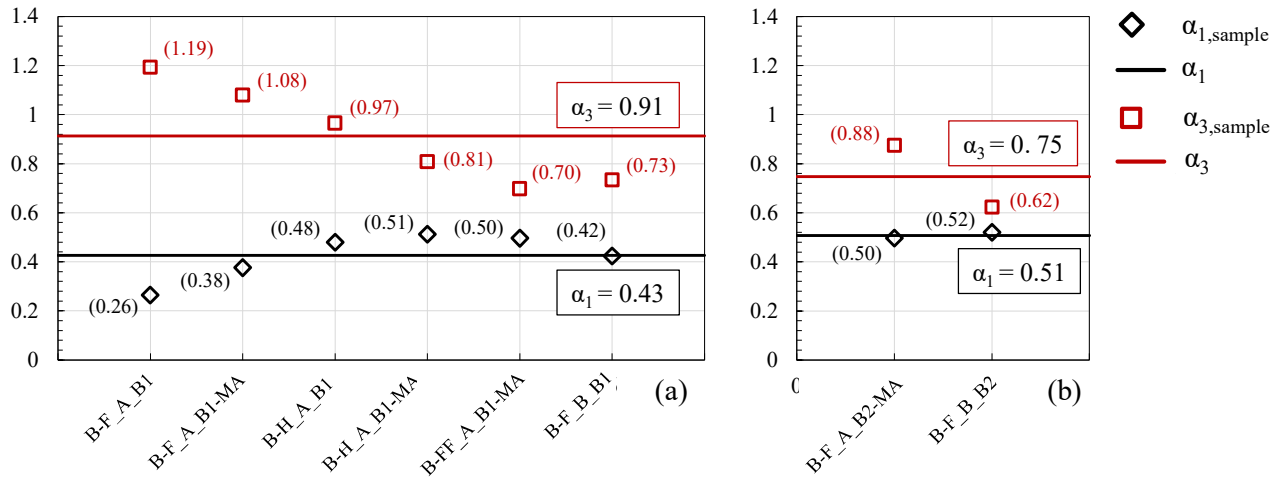

Figure 14. Evaluation of the compatibility coefficients α_i: (a) samples strengthened by grid B1; (b) samples strengthened by grid B2.

Considering that the two investigated masonry typologies can be both classified as clay brick masonry with lime-based mortar and that a similar shear behavior was observed for the URM samples, a mean value of the coefficient α_1 was obtained for every different type of reinforcement, irrespective of the type of masonry. Correspondingly, values proposed for the coefficient α_1 were equal to 0.43 (CoV = 22.0%) and 0.51 (CoV = 3.3%) for the panels strengthened with the basalt grid B1 and B2, respectively. The corresponding values of the coefficient α_2 were equal to 0.09 (CoV = 22.0%) and 0.10 (CoV = 3.3%). For the calibration of the coefficient α_3, a single average value can be proposed for each FRCM strengthening system. In particular, the following values of the coefficient α_3 were determined for bidirectional basalt grids: 0.91 (CoV = 14.4%) for grid B1 and 0.75 (CoV = 21.9%) for grid B2. Values of the compatibility coefficients α_1 and α_3, for the investigated masonry typologies and FRCM strengthening systems (all the samples) are graphically presented in Figure 14, together with their average values (solid lines). Values of the compatibility

factors are not proposed for the bidirectional aramid-glass grids (AG), since they would be based on single results and, therefore, cannot be considered reliable and representative of the contribution of these reinforcing systems, for which further studies are recommended. Worth mentioning that the value of the coefficient α_3 obtained for the grid B2 is similar to the strength reduction factors proposed in the analytical formulations reported in Section 2 [52,53], while the value obtained for the grid B1 is slightly higher. In Table 7, the fiber contribution P_f and the theoretical value of the second peak load $P_{2,th}$, evaluated according to Equation (13) by using the calibrated compatibility factors, are reported together with the error with respect to the experimental results ($P_{2,exp.}$). The value of $P_{2,th}$ is presented also for the sample B-F_B_AG-1 and it was calculated by using the compatibility factors determined for the grid B2, given the similar axial stiffness of the composite systems (Figure 8). The error, in this case, was slightly higher with respect to the other samples, but still acceptable.

The proposed approach is purposely maintained sufficiently simple and based on the evaluation of a limited number of mechanical parameters through standard experimental tests. Even if it was defined starting from the observations obtained in diagonal compression tests, it is suggested to use it also for the evaluation of the shear capacity of existing masonry structural elements, strengthened through composite systems. The approach can be adopted in the design of strengthening interventions on masonry piers (with the appropriate safety factors), where, even if the first peak load is usually the maximum one, it is important to evaluate both the load capacities P_1 and P_2.

7 Conclusions

In this paper, the shear behavior of FRCM/SRG strengthened masonry panels was investigated both from the experimental and the analytical point of view, with two main objectives: (i) to analyze the efficiency of different composite systems in improving the shear behavior of brick masonry panels, and (ii) to propose an analytical approach applicable for the prediction of the shear strength increase expected for strengthened masonry panels.

Experimentally, diagonal compression tests were performed on 17 samples, built with different materials and bond patterns with the aim of reproducing typical masonry typologies of the Italian territory. 13 samples were then reinforced through various strengthening systems, differing in the materials adopted, i.e. basalt, glass or steel, and in the fibers arrangements, i.e. unidirectional or bidirectional, continuous or discontinuous. The experimental results allowed to draw the following conclusions:

- The application of the investigated composite systems did influence the shear capacity of the masonry panels, producing significant strength increments for all the investigated masonry typologies, generally higher for continuous strengthening layouts.
- The shear behavior of FRCM/SRG strengthened samples was characterized by a first peak load, corresponding to the macroscopic cracking of the mortar matrix, and by a second peak load, corresponding to the failure of the fibers; in most of the tests, the maximum load coincided with the first peak load.
- The presence of the composite systems did not produce a significant increase in the shear stiffness of the samples, confirming the ability of these materials to improve the shear behavior without determining considerable variations in the stiffness distribution of existing buildings.
- The pseudo-ductility of the FRCM/SRG strengthened samples was evaluated to quantitively assess the significant role of the fibers in reducing the brittleness of the shear failure; the displacement capacity of the FRCM/SRG strengthened samples was, indeed, significantly higher than the one of the unreinforced samples.

An important outcome of the experimental campaign was related to the fact that, in most of the tests, the cracking of the mortar matrix corresponded to the capacity of the strengthened masonry panels. For this reason, an analytical approach for the evaluation of the shear capacity of strengthened masonry panels was here proposed including the mortar matrix contribution, which is not taken into account by most of the formulations available to date. The proposed approach, described for

continuous and symmetric reinforcements, implies the determination of the two peak loads observed experimentally, one associated to the cracking of the mortar matrix and one associated to the failure of the reinforcements. It was calibrated and validated through comparison with the experimental results and it can also be adopted for the prediction of the shear capacity of strengthened masonry structural elements. Further experimental campaigns could be conducted and a wider experimental database could be considered to extend the validity and the robustness of the proposed formulation to different FRCM/SRG strengthening systems.

8 Acknowledgments

The financial and technical support of the Kerakoll Company, Sassuolo (Modena, Italy), and the financial support of the Italian Department of Civil Protection (ReLUIS 2020 Grant – Innovative Materials) are gratefully acknowledged. Mr. Diiterihs Erra, Mr. Michele Esposito (Technical staff at CIRI Buildings & Construction) and the master students Giulia Palmieri and Ylenia Leonardi are gratefully acknowledged for their work during the setup of the tests.

References

[1] Ceci AM, Contento A, Fanale L, Galeota D, Gattulli V, Lepidi M, et al. Structural performance of the historic and modern buildings of the University of L'Aquila during the seismic events of April 2009. Eng Struct 2010;32:1899–924. https://doi.org/10.1016/j.engstruct.2009.12.023.

[2] Indirli M, Kouris SLA, Formisano A, Borg RP, Mazzolani FM. Seismic Damage Assessment of Unreinforced Masonry Structures After The Abruzzo 2009 Earthquake: The Case Study of the Historical Centers of L'Aquila and Castelvecchio Subequo. Int J Archit Herit 2013;7:536–78. https://doi.org/10.1080/15583058.2011.654050.

[3] Penna A, Morandi P, Rota M, Manzini CF, da Porto F, Magenes G. Performance of masonry buildings during the Emilia 2012 earthquake. Bull Earthq Eng 2014;12:2255–73. https://doi.org/10.1007/s10518-013-9496-6.

[4] Lagomarsino S. On the vulnerability assessment of monumental buildings. Bull Earthq Eng 2006;4:445–63. https://doi.org/10.1007/s10518-006-9025-y.

[5] Rota M, Penna A, Strobbia CL. Processing Italian damage data to derive typological fragility curves. Soil Dyn Earthq Eng 2008;28:933–47. https://doi.org/10.1016/j.soildyn.2007.10.010.

[6] Ferretti F, Ferracuti B, Mazzotti C, Savoia M. Destructive and minor destructive tests on masonry buildings: Experimental results and comparison between shear failure criteria. Constr Build Mater 2019;199:12–29. https://doi.org/10.1016/j.conbuildmat.2018.11.246.

[7] Corradi M, Borri A, Vignoli A. Experimental Evaluation of In-plane Shear Behaviour of Masonry Walls Retrofitted Using Conventional and Innovative Methods. Mason Int 2008;21:29–41.

[8] Valluzzi MR. Challenges and perspectives for the protection of masonry structures in historic centers: the role of innovative materials and techniques. RILEM Tech Lett 2016;1:45. https://doi.org/10.21809/rilemtechlett.v1.10.

[9] Marcari G, Oliveira D V, Fabbrocino G, Lourenço PB. Shear capacity assessment of tuff panels strengthened with FRP diagonal layout. Compos Part B Eng 2011;42:1956–65. https://doi.org/10.1016/j.compositesb.2011.05.031.

[10] Valluzzi MR, Tinazzi D, Modena C. Shear behavior of masonry panels strengthened by FRP laminates. Constr Build Mater 2002;16:409–16. https://doi.org/10.1016/S0950-0618(02)00043-0.

[11] Ferretti F, Incerti A, Ferracuti B, Mazzotti C. Diagonal compression tests on masonry panels strengthened by FRP and FRCM. Struct. Anal. Hist. Constr. Anamn. diagnosis, Ther. Control. - Proc. 10th Int. Conf. Struct. Anal. Hist. Constr., 2016. https://doi.org/10.1201/9781315616995-159.
[12] Alecci V, Barducci S, D'Ambrisi A, De Stefano M, Focacci F, Luciano R, et al. Shear capacity of masonry panels repaired with composite materials: Experimental and analytical investigations. Compos Part B Eng 2019;171:61–9. https://doi.org/10.1016/j.compositesb.2019.04.013.
[13] Shrive NG. The use of fibre reinforced polymers to improve seismic resistance of masonry. Constr Build Mater 2006;20:269–77. https://doi.org/10.1016/j.conbuildmat.2005.08.030.
[14] Fedele R, Milani G. A numerical insight into the response of masonry reinforced by FRP strips. The case of perfect adhesion. Compos Struct 2010;92:2345–57. https://doi.org/10.1016/j.compstruct.2010.03.014.
[15] Valluzzi MR, Oliveira D V., Caratelli A, Castori G, Corradi M, de Felice G, et al. Round Robin Test for composite-to-brick shear bond characterization. Mater Struct 2012;45:1761–91. https://doi.org/10.1617/s11527-012-9883-5.
[16] Ceroni F, de Felice G, Grande E, Malena M, Mazzotti C, Murgo F, et al. Analytical and numerical modeling of composite-to-brick bond. Mater Struct 2014;47:1987–2003. https://doi.org/10.1617/s11527-014-0382-8.
[17] Mazzotti C, Ferracuti B, Bellini A. Experimental Study on Masonry Panels Strengthened by GFRP: The Role of Inclination between Mortar Joints and GFRP Sheets. Key Eng Mater 2014;624:559–66. https://doi.org/10.4028/www.scientific.net/KEM.624.559.
[18] Mazzotti C, Sassoni E, Bellini A, Ferracuti B, Franzoni E. Strengthening of Masonry Elements by FRP: Influence of Brick Mechanical and Microstructural Properties. Key Eng Mater 2014;624:330–7. https://doi.org/10.4028/www.scientific.net/KEM.624.330.
[19] Sassoni E, Sarti V, Bellini A, Mazzotti C, Franzoni E. The role of mortar joints in FRP debonding from masonry. Compos Part B Eng 2018;135:166–74. https://doi.org/10.1016/j.compositesb.2017.10.021.
[20] Papanicolaou CG, Triantafillou TC, Papathanasiou M, Karlos K. Textile reinforced mortar (TRM) versus FRP as strengthening material of URM walls: out-of-plane cyclic loading. Mater Struct 2007;41:143–57. https://doi.org/10.1617/s11527-007-9226-0.
[21] Papanicolaou CG, Triantafillou TC, Karlos K, Papathanasiou M. Textile-reinforced mortar (TRM) versus FRP as strengthening material of URM walls: in-plane cyclic loading. Mater Struct 2007;40:1081–97. https://doi.org/10.1617/s11527-006-9207-8.
[22] Papanicolaou C, Triantafillou T, Lekka M. Externally bonded grids as strengthening and seismic retrofitting materials of masonry panels. Constr Build Mater 2011;25:504–14. https://doi.org/10.1016/j.conbuildmat.2010.07.018.
[23] de Felice G, Aiello MA, Bellini A, Ceroni F, De Santis S, Garbin E, et al. Experimental characterization of composite-to-brick masonry shear bond. Mater Struct Constr 2016;49:2581–96. https://doi.org/10.1617/s11527-015-0669-4.
[24] Carozzi FG, Bellini A, D'Antino T, de Felice G, Focacci F, Hojdys Ł, et al. Experimental investigation of tensile and bond properties of Carbon-FRCM composites for strengthening masonry elements. Compos Part B Eng 2017;128:100–19. https://doi.org/10.1016/j.compositesb.2017.06.018.
[25] Caggegi C, Carozzi FG, De Santis S, Fabbrocino F, Focacci F, Hojdys Ł, et al. Experimental analysis on tensile and bond properties of PBO and aramid fabric reinforced cementitious matrix for strengthening masonry structures. Compos Part B Eng 2017;127:175–95. https://doi.org/10.1016/j.compositesb.2017.05.048.
[26] Leone M, Aiello MA, Balsamo A, Carozzi FG, Ceroni F, Corradi M, et al. Glass fabric reinforced cementitious matrix: Tensile properties and bond performance on masonry substrate. Compos Part B Eng 2017;127:196–214. https://doi.org/10.1016/j.compositesb.2017.06.028.
[27] Lignola GP, Caggegi C, Ceroni F, De Santis S, Krajewski P, Lourenço PB, et al. Performance assessment of basalt FRCM for retrofit applications on masonry. Compos Part B Eng 2017;128:1–18. https://doi.org/10.1016/j.compositesb.2017.05.003.
[28] de Felice G, Aiello MA, Caggegi C, Ceroni F, De Santis S, Garbin E, et al. Recommendation of RILEM Technical Committee 250-CSM: Test method for Textile Reinforced Mortar to substrate bond characterization. Mater Struct 2018;51:95. https://doi.org/10.1617/s11527-018-1216-x.
[29] Bellini A, Bovo M, Mazzotti C. Experimental and numerical evaluation of fiber-matrix interface behaviour of different FRCM systems. Compos Part B Eng 2019;161:411–26. https://doi.org/10.1016/j.compositesb.2018.12.115.
[30] Bellini A, Shahreza SK, Mazzotti C. Cyclic bond behavior of FRCM composites applied on masonry substrate. Compos Part B Eng 2019;169:189–99. https://doi.org/10.1016/j.compositesb.2019.04.009.
[31] Bellini A, Mazzotti C. Bond Behavior of FRCM Composites Applied on Concrete and Masonry, 2020, p. 347–59. https://doi.org/10.1007/978-3-030-23748-6_27.
[32] De Santis S, Ceroni F, de Felice G, Fagone M, Ghiassi B, Kwiecień A, et al. Round Robin Test on tensile and bond behaviour of Steel Reinforced Grout systems. Compos Part B Eng 2017;127:100–20. https://doi.org/10.1016/j.compositesb.2017.03.052.
[33] Bellini A, Incerti A, Mazzotti C. Out-of-Plane Strengthening of Masonry Walls with FRCM Composite Materials.

Key Eng Mater 2017;747:158–65. https://doi.org/10.4028/www.scientific.net/KEM.747.158.
[34] Bellini A, Incerti A, Bovo M, Mazzotti C. Effectiveness of FRCM Reinforcement Applied to Masonry Walls Subject to Axial Force and Out-Of-Plane Loads Evaluated by Experimental and Numerical Studies. Int J Archit Herit 2018;12:376–94. https://doi.org/10.1080/15583058.2017.1323246.
[35] Murgo FS, Mazzotti C. Masonry columns strengthened with FRCM system: Numerical and experimental evaluation. Constr Build Mater 2019;202:208–22. https://doi.org/10.1016/j.conbuildmat.2018.12.211.
[36] Del Zoppo M, Di Ludovico M, Prota A. Analysis of FRCM and CRM parameters for the in-plane shear strengthening of different URM types. Compos Part B Eng 2019;171:20–33. https://doi.org/10.1016/j.compositesb.2019.04.020.
[37] Babaeidarabad S, De Caso F, Nanni A. URM Walls Strengthened with Fabric-Reinforced Cementitious Matrix Composite Subjected to Diagonal Compression. J Compos Constr 2014;18:04013045. https://doi.org/10.1061/(ASCE)CC.1943-5614.0000441.
[38] Ferretti F, Incerti A, Ferracuti B, Mazzotti C. FRCM Strengthened Masonry Panels: The Role of Mechanical Anchorages and Symmetric Layouts. Key Eng Mater 2017;747:334–41. https://doi.org/10.4028/www.scientific.net/KEM.747.334.
[39] Incerti A, Tilocca AR, Ferretti F, Mazzotti C. Influence of Masonry Texture on the Shear Strength of FRCM Reinforced Panels. RILEM Bookseries, vol. 18, 2019, p. 1623–31. https://doi.org/10.1007/978-3-319-99441-3_174.
[40] Del Zoppo M, Di Ludovico M, Balsamo A, Prota A. Experimental In-Plane Shear Capacity of Clay Brick Masonry Panels Strengthened with FRCM and FRM Composites. J Compos Constr 2019;23:04019038. https://doi.org/10.1061/(ASCE)CC.1943-5614.0000965.
[41] Prota A, Marcari G, Fabbrocino G, Manfredi G, Aldea C. Experimental In-Plane Behavior of Tuff Masonry Strengthened with Cementitious Matrix–Grid Composites. J Compos Constr 2006;10:223–33. https://doi.org/10.1061/(ASCE)1090-0268(2006)10:3(223).
[42] Parisi F, Iovinella I, Balsamo A, Augenti N, Prota A. In-plane behaviour of tuff masonry strengthened with inorganic matrix–grid composites. Compos Part B Eng 2013;45:1657–66. https://doi.org/10.1016/j.compositesb.2012.09.068.
[43] Bilotta A, Ceroni F, Nigro E, Pecce M. Experimental tests on FRCM strengthening systems for tuff masonry elements. Constr Build Mater 2017;138:114–33. https://doi.org/10.1016/j.conbuildmat.2017.01.124.
[44] Marcari G, Basili M, Vestroni F. Experimental investigation of tuff masonry panels reinforced with surface bonded basalt textile-reinforced mortar. Compos Part B Eng 2017;108:131–42. https://doi.org/10.1016/j.compositesb.2016.09.094.
[45] Feo L, Luciano R, Misseri G, Rovero L. Irregular stone masonries: Analysis and strengthening with glass fibre reinforced composites. Compos Part B Eng 2016;92:84–93. https://doi.org/10.1016/j.compositesb.2016.02.038.
[46] Ferretti F, Incerti A, Tilocca AR, Mazzotti C. In-Plane Shear Behavior of Stone Masonry Panels Strengthened through Grout Injection and Fiber Reinforced Cementitious Matrices. Int J Archit Herit 2019:1–20. https://doi.org/10.1080/15583058.2019.1675803.
[47] Guerreiro J, Proença J, Ferreira JG, Gago A. Experimental characterization of in-plane behaviour of old masonry walls strengthened through the addition of CFRP reinforced render. Compos Part B Eng 2018;148:14–26. https://doi.org/10.1016/j.compositesb.2018.04.045.
[48] Bellini A, Tilocca AR, Frana I, Savoia M, Mazzotti C. Environmental durability of FRCM strengthening systems and comparison with dry fabrics. In: Taylor&FrancisGroup, London, editor. Brick Block Mason. -From Hist. to Sustain. Mason., Krakow, Poland: 2020, p. 370–8.
[49] Donnini J, Bompadre F, Corinaldesi V. Tensile Behavior of a Glass FRCM System after Different Environmental Exposures. Processes 2020;8:1074. https://doi.org/10.3390/pr8091074.
[50] Dalalbashi A, Ghiassi B, Oliveira D V. Aging of lime-based TRM composites under natural environmental conditions. Constr Build Mater 2021;270:121853. https://doi.org/10.1016/j.conbuildmat.2020.121853.
[51] CNR-DT 200 R1. Guide for the Design and Construction of Externally Bonded FRP Systems for Strengthening Existing Structures. National Research Council (CNR); 2013.
[52] ACI 549.6R-20. Design and construction of externally bonded Fabric-Reinforced Cementitious Matrix (FRCM) systems for repair and strengthening concrete and masonry Structures. American Concrete Instutute (ACI); 2020.
[53] CNR-DT 215/2018. Istruzioni per la Progettazione, l'Esecuzione ed il Controllo di Interventi di Consolidamento Statico mediante l'utilizzo di Compositi Fibrorinforzati a Matrice Inorganica (in Italian). National Research Council (CNR); 2018.
[54] Ascione L, Carozzi FG, D'Antino T, Poggi C. New Italian guidelines for design of externally bonded Fabric-Reinforced Cementitious Matrix (FRCM) systems for repair and strengthening of masonry and concrete structures. Procedia Struct Integr 2018;11:202–9. https://doi.org/10.1016/j.prostr.2018.11.027.
[55] Faella C, Martinelli E, Nigro E, Paciello S. Shear capacity of masonry walls externally strengthened by a cement-based composite material: An experimental campaign. Constr Build Mater 2010;24:84–93. https://doi.org/10.1016/j.conbuildmat.2009.08.019.
[56] Gattesco N, Boem I. Experimental and analytical study to evaluate the effectiveness of an in-plane reinforcement

for masonry walls using GFRP meshes. Constr Build Mater 2015;88:94–104. https://doi.org/10.1016/j.conbuildmat.2015.04.014.
[57] Gattesco N, Boem I. Influence of mortar coating type on the shear resistance of a GFRP based strengthening technique for brick masonry walls. Brick Block Mason Trends, Innov Challenges - Proc 16th Int Brick Block Mason Conf IBMAC 2016 2016:403–10. https://doi.org/10.1201/b21889-48.
[58] Incerti A, Ferretti F, Mazzotti C. FRCM strengthening systems efficiency on the shear behavior of pre-damaged masonry panels: an experimental study. J Build Pathol Rehabil 2019;4:14. https://doi.org/10.1007/s41024-019-0053-9.
[59] D'Antino T, Carozzi FG, Poggi C. Diagonal shear behavior of historic walls strengthened with composite reinforced mortar (CRM). Mater Struct 2019;52:114. https://doi.org/10.1617/s11527-019-1414-1.
[60] Gattesco N, Boem I. Experimental and analytical study to evaluate the effectiveness of an in-plane reinforcement for masonry walls using GFRP meshes. Constr Build Mater 2015;88:94–104. https://doi.org/10.1016/j.conbuildmat.2015.04.014.
[61] EN 772-1. Methods of test for masonry units - Part 1: Determination of compressive strength 2011.
[62] EN 12390-6:2009. Testing hardened concrete - Part 6: Tensile splitting strength of test specimen 2010.
[63] EN 12390-5:2009. Testing hardened concrete - Part 5: Flexural strength of test specimens 2009.
[64] EN 12390-13. Testing hardened concrete - Determination of secant modulus of elasticity in compression 2013.
[65] EN 1015-11:1999/A1:2006. Methods of test for mortar for masonry - Part 11: Determination of flexural and compressive strength of hardened mortar 2006.
[66] Linea Guida per la identificazione, la qualificazione ed il controllo di accettazione di compositi fibrorinforzati a matrice inorganica (FRCM) da utilizzarsi per il consolidamento strutturale di costruzioni esistenti (in italian). Consiglio Superiore dei Lavori Pubblici; 2018.
[67] Santandrea M, Imohamed IAO, Carloni C, Mazzotti C, de Miranda S, Ubertini F. A study of the debonding mechanism in steel and basalt FRCM-masonry joints. Brick Block Mason. Trends, Innov. Challenges - Proc. 16th Int. Brick Block Mason. Conf. IBMAC 2016, 2016, p. 433–40.
[68] ASTM E519−15. Standard test method for diagonal tension (shear) in masonry assemblages 2015:4–8. https://doi.org/10.1520/E0519.
[69] RILEM MS - D6. In situ measurement of masonry bed joint shear strength 1996.
[70] Frocht M. Recent advances in photoelasticity. ASME Trans 1931;55:135–53.
[71] Yokel FY, Fattal SG. A Failure hypothesis for masonry shearwalls. J Struct Div - ASCE 1976;102:515–32.
[72] Calderini C, Cattari S, Lagomarsino S. The use of the diagonal compression test to identify the shear mechanical parameters of masonry. Constr Build Mater 2010;24:677–85. https://doi.org/10.1016/j.conbuildmat.2009.11.001.
[73] EN1992-1-1:2004+A1:2014. Eurocode 2: Design of concrete structures - Part 1-1: General rules and rules for buildings 2014.